RSC Advances

ROYAL SOCIETY OF CHEMISTRY

www.rsc.org/advances

Cite this: DOI: 10.1039/c0xx00000x

www.rsc.org/xxxxxx

ARTICLE TYPE

$K_2TiO(C_2O_4)_2$-mediated synthesis of rutile TiO_2 mesocrystals and their ability to assist photodegradation of sulfosalicylic acid in water

Lu-Lu Lai [a] **and Jin-Ming Wu*** [a]

Received (in XXX, XXX) Xth XXXXXXXXX 20XX, Accepted Xth XXXXXXXXX 20XX

DOI: 10.1039/b000000x

Flower-like rutile TiO_2 mesocrystals were fabricated by a $K_2TiO(C_2O_4)_2$-mediated Ti-H_2O_2 interaction at 80 °C and under the atmospheric pressure. Both thin films precipitated on the metallic Ti substrates and powders collected from the solutions were subjected to detailed characterizations in nanostructures and photocatalytic performances. The Ti-H_2O_2 interaction at 80 °C resulted in arrays of hydrogen titanate nanowires on Ti substrates and the corresponding nanowires in the solution as well. With the additive of $K_2TiO(C_2O_4)_2$, flower-like rutile TiO_2 mesocrystals appeared via an oriented attachment self-assembly approach. The hydrogen titanate nanowires decomposed to anatase TiO_2 nanowires when heated in air at 450 °C; whilst the rutile TiO_2 mesocrystals remained unchanged upon the subsequent calcination. The photocatalytic activity of both thin films and powders after the calcination was evaluated by photodegradation of sulfosalicylic acid (SSA) in water under the UV light illumination. It was found that anatase favored the degradation of SSA than rutile; however, the larger specific surface area of mesocrystals, as well as the high charge separation rate inherent from their single crystal nature, compensated effectively the photocatalytic performance for the flower-like rutile TiO_2 mesocrystals.

Introduction

Increasing attention has been paid to photocatalysts with high performances for water and air remediation.[1] Titanium dioxide (TiO_2), which is an n-type wide bandgap semiconductor, has been widely investigated since the discovery of its ability for photocatalytic water splitting under a bias potential.[2] For decades, significant efforts have been devoted to clarify the exact mechanisms of the photocatalytic reactions involving TiO_2, considering mainly the various effects of dopants, nanostructures, crystal phases, and surface states.[3] Up to now, titania with various nanostructures has been fabricated, such as microspheres,[4] nanotubes,[5] nanowires,[6] nanorods,[7] nanosheets,[8] nanoflowers,[9] and hierarchically structures[10] constructed from them.

Mesoscopically structured crystals, also known as mesocrystals, are colloidal crystals built up from individual nanocrystals that align in a common crystallographic structure to form porous quasi-single crystals.[11] There is a flourishing emergence of mesocrystals related to various materials, including metal oxides,[12] metals,[13] calcium carbonate,[14] and so forth, because mesocrystals not only possess similar properties as single crystals but also show large specific surface area.[15] Not surprisingly, TiO_2 mesocrystals have been commonly reported, via mainly hydrothermal[16] or solvothermal appraches.[17] For example, Hong et al.[18] synthesized titanate nanowires via a hydrothermal procedure. A subsequent treatment in an acidic aqueous solution for 7 days resulted in rutile TiO_2 mesocrystals. Recently, Aoyama et al. synthesized mesocrystal nanosheets of rutile TiO_2 on a glass slide via a heterogeneous nucleation and growth procedure simply in a $TiCl_3$ aqueous solution.[19] Silva et al. prepared anatase TiO_2 mesocrystals via a non-aqueous sol-gel synthetic method involving the reaction of $TiCl_4$ and *n*-octanol.[20] Several Ti-based precursors, such as titanium glycolate[21] and sodium fluorotitanates,[22] have been developed to fabricate TiO_2 nanowires, nanoparticles, or polyhedra. Among them, NH_4TiOF_3 can be converted to TiO_2 mesocrystals.[23] So far, to synthesize TiO_2 mesocrystals under a low temperature and the atmospheric pressure is of interest yet rarely reported.

Our previous studies reported that titanate nanowires can be achieved simply by oxidations of metallic Ti with aqueous H_2O_2 solutions which contain certain amounts of HNO_3 and melamine, under a low temperature of 80 °C and the atmospheric pressure.[6a,24] Herein, we report our finding that rutile TiO_2 mesocrystal nanoflowers can be achieved simply by the additive of $K_2TiO(C_2O_4)_2$ in the solution. The products, in forms of both thin films and powders, were applied as photocatalysts to assist the photodegradation of sulfosalicylic acid (SSA) in water and the photocatalytic activity was correlated to the structural parameters.

Experimental section

Synthesis

Titanium plates with the size of 2.5 cm × 3.5 cm × 0.01 cm were etched in a mixture of 55 wt. % HF, 63 wt. % HNO_3 and distilled water, in a volume ration of 1:3:6 for 30 seconds, followed by cleaning in distilled water with an ultrasonic bath. Each cleaned Ti plate was placed at an angle against the wall of a beaker, totally immersed in 17.5 mL 10 wt. % H_2O_2 solution, which contained 2.4 M melamine ($C_3H_6N_6$) and 0.29 M HNO_3, and kept for 72 h in an oven maintained at 80 °C. The H_2O_2 solution containing $C_3H_6N_6$ and HNO_3 is simplified as the H_2O_2 solution hereafter. Into the H_2O_2 solution, 0, 50 and 100 mM $K_2TiO(C_2O_4)_2$ were added to control the reaction products. The

reacted Ti plates were rinsed gently in distilled water while the precipitates were collected by centrifugations, which were then washed several times with distilled water and absolute ethanol sequentially, and finally dried at 80 °C in an oven overnight. The obtained plates and powders were further subjected to a final calcination in air at 450 °C for 1 h.

Characterization

The morphologies of the samples were examined by a field-emission scanning electron microscopy (FESEM, Hitachi, S–4800) and a transmission electron microscopy (TEM, JEOL, JEM–2010). The X-ray diffraction (XRD) tests were performed using a Rigaku D/max-3B diffractometer with CuKα radiation, operated at 40 kV, 36 mA (λ = 0.15406 nm). The UV–Vis diffuse reflectance spectra were measured using a UV–Vis near-infrared spectrometer (UV–3150, Shimadzu). Nitrogen sorption measurements were conducted at 77 K using a Nova 3000e (Quantachrome Instruments, USA) with a Quantachrome V11.0 software. The Brunauer-Emmett-Teller (BET) approach using desorption data and the relative pressure below 0.3 was utilized to determine the surface area. The pore size distribution and pore volume were estimated by the Barrett-Joyner-Halenda (BJH) method using the desorption curve. The sample was degassed at 150 °C to remove physisorbed gases prior to the measurement.

Photocatalytic test

The photocatalytic activities of both thin films and powders after calcinations were evaluated by degradation of SSA with an initial concentration of 10 mg/L, under UV light illumination. A 50 mL SSA solution in the presence of the photocatalyst (2.5 × 2.5 cm^2 for films and 25 mg for powders) was firstly stirred in the dark for 120 min to reach an absorption-desorption equilibrium and then subjected to a UV lamp illumination for up to 120 min. The average intensity of the UV irradiance reaching the sample was measured to be ca. 5.3 mW/cm^2, using an irradiance meter (Model: UV–A, Beijing Normal University, China, measured for the wavelength range from 320–400 nm with a peak wavelength of 365 nm). The SSA concentration was monitored with a UV–Vis spectrophotometer (UV–1800PC, Shanghai Mapada) at the wavelength of 208 nm. For the slurry system, the SSA concentration was determined after removing the powders by centrifugations.

Results and Discussion

Figure 1 shows the surface and cross sectional FESEM morphologies of thin films on Ti plates, which were achieved by varying the amounts of $K_2TiO(C_2O_4)_2$. Quasi-aligned nanowires can be seen covering thoroughly the Ti plate after the oxidation at 80 °C for 72 h with the H_2O_2 solution (**Fig. 1**a, b). A compact intermediate layer can be observed between the nanowires and the Ti substrate. The average length of the nanowires was *ca*. 2.0 μm and the total film thickness was *ca*. 4.0 μm (**Fig. 1**c). With the additive of 50 mM $K_2TiO(C_2O_4)_2$ in the H_2O_2 solution, flower-like structures appeared together with the nanowires (**Fig. 1**d, e). The total film thickness reduced to be *ca*. 2.1 μm (**Fig. 1**f) and the top layer became more compact when compared with the nanowire layer. Further increasing the concentration of $K_2TiO(C_2O_4)_2$ to 100 mM resulted in the disappearance of the distinguishable nanowires. Only dispersed nanoflowers with an average petal length of 160 nm and width of 60 nm can be seen in **Fig. 1**g, h. Further heating these films at 450 °C in air for 1 h wouldn't change the film structure. **Fig. 2** indicates that, all the powders collected from the solutions after the reactions possessed the same structures as those in the corresponding thin films.

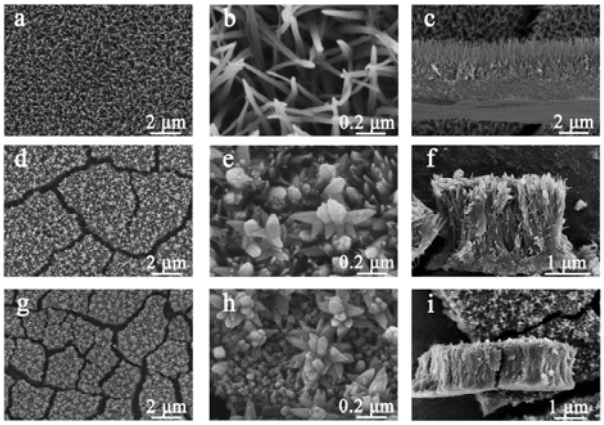

Fig. 1 FESEM morphologies of thin films achieved by the reaction between a Ti plate and the H_2O_2 solution with (a, b, c) 0 mM, (d, e, f) 50 mM and (g, h, i) 100 mM of $K_2TiO(C_2O_4)_2$.

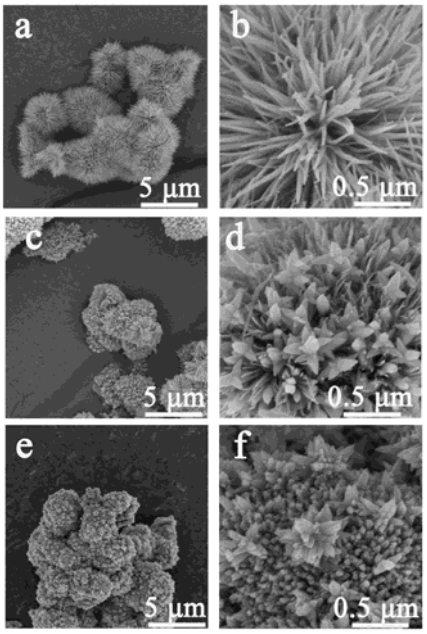

Fig. 2 FE-SEM morphologies of the powders collected from the solution achieved by the reaction between a Ti plate and the H_2O_2 solution with (a, b) 0 mM, (c, d) 50 mM and (e, f) 100 mM. The powders were subjected to calcination at 450 °C for 1 h.

Figure 3 demonstrates the XRD patterns of both the powders and films, before and after calcinations in air at 450 °C for 1 h. The as-synthesized nanowires could be indexed to pentatitanate $H_2Ti_5O_{11}\cdot 3H_2O$ (JCPDS card 44-0130) by showing a strong diffraction peak at $2\theta = 8.4^o$ (**Fig. 3**a), which crystallized mainly to anatase (JCPDS card 21-1272) along with small amounts of srilankite (JCPDS card 21-1236) after the thermal treatment (**Fig. 3**b). With the appearance of nanoflowers, the powders exhibited XRD patterns corresponding to rutile (JCPDS card 21-1276) even

before the thermal treatment, indicating the direct crystallization of rutile at a temperature as low as 80 °C (50 mM and 100 mM, **Fig. 3**a). For the powders collected from the solution with the additive of 50 mM $K_2TiO(C_2O_4)_2$ and after calcinating at 450 °C for 1 h, the XRD pattern demonstrates the peaks corresponding to anatase, srilankite and rutile. Anatase and srilankite resulted from decompositions of the pentatitanate nanowires; whilst rutile came from the nanoflowers. When the concentration of $K_2TiO(C_2O_4)_2$ further increased to 100 mM, which led to the total disappearance of the distinguishable nanowires, only anatase and rutile can be detected after the calcination. The absence of srilankite in this sample is in accordance with the FESEM observation that nanowires are absent (**Fig. 1**g-i), because pentatitanate nanowires decomposed to anatase with trace srilankite. Here, the anatase phase came from the crystallized nanoparticulate aggregates and the rutile phase came from the nanoflowers.

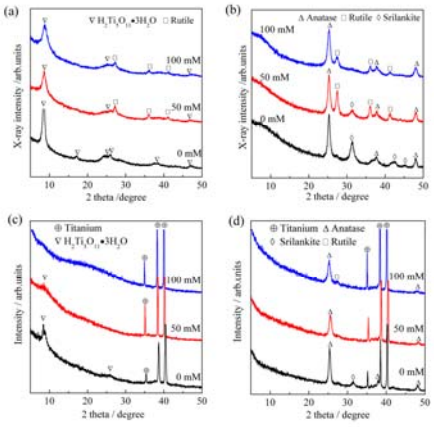

Fig. 3 XRD patterns of (a) powders and (c) thin films achieved by the reaction between a Ti plate and the H_2O_2 solution with various amounts of $K_2TiO(C_2O_4)_2$. The corresponding powders and films after calcination in air at 450 °C for 1 h are illustrated in (b) and (d), respectively.

For the calcinated thin films (**Fig. 3**c, d), XRD peaks other than anatase are overshadowed by the strong peaks arising from the metallic Ti substrates. However, the results support the aforementioned analysis that the as-synthesized nanoflowers are rutile; whilst the as-synthesized nanowires are pentatitanate that decomposed to anatase and trace srilankite after calcinating at 450 °C for 1 h in air. At present time, we are unable to obtain thin films or powders consisted of mesocrystals only.

Figure 4a illustrates a typical TEM image of powders achieved with the additive of 50 mM $K_2TiO(C_2O_4)_2$ in the H_2O_2 solution, of which nanowires and nanoflowers coexisted. The internal porosity is revealed by the TEM image, which clearly displays mesopores inside the single-crystals. The high resolution TEM (HRTEM) image shown in **Fig. 4**b further confirms that the calcinated nanowires consisted of anatase and srilankite. As suggested by the HRTEM image in **Fig. 4**c, the calcinated nanoflowers consisted of rutile TiO_2 with mesopores. More interestingly, the corresponding selected area electron diffraction (SAED) pattern (**Fig. 4**d) exhibits "single-crystal-like" diffraction spots corresponding to rutile TiO_2, indicating further the formation of a mesocrystal structure. According to the literature, the porous structure combined with the single crystal character is typical for mesocrystals constructed through an oriented self-assemble process.[11] The rutile mesocrystals grew along the [001] direction, which can be contributed to the diversity in the growth rate along various facets. For rutile, the sequence is (110) < (100) < (101) < (001). In this way, the TiO_6 octahedron shares edges with each other and develops to from the rutile mesocrystals along the [001] direction.[25]

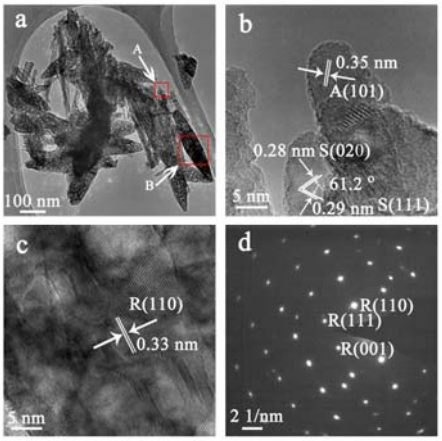

Fig. 4 TEM images of the powders derived by the reaction between a Ti plate and the H_2O_2 solution with 50 mM $K_2TiO(C_2O_4)_2$. (a) TEM image; (b and c) HRTEM images of region A and B as labelled in (a), respectively; (d) the corresponding SAED pattern of (c). The powders were subjected to a final calcination in air at 450 °C for 1 h.

The N_2 adsorption-desorption isotherms and pore size distribution of the calcinated powders are shown in **Fig. 5** and the calculated data are listed in **Table 1**. An IV type isotherm with a H3 type hysteresis loop, which demonstrates a mesoporous structure,[26] can be discerned, especially for the powders achieved with the additive of 100 mM $K_2TiO(C_2O_4)_2$. The specific surface area increased with increasing $K_2TiO(C_2O_4)_2$ concentrations. The diameter of nanopores estimated from the TEM image in **Fig. 4**a is between 3–8 nm, which agrees well with the pore size distribution as illustrated in **Fig. 5**b.

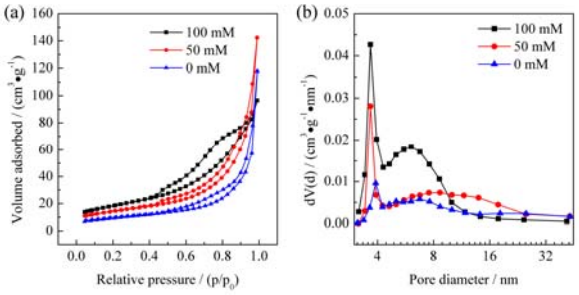

Fig. 5 The N_2 adsorption-desorption isotherms (a) and the pore size distribution curve (b) of the powders derived by the reaction between a Ti plate and the H_2O_2 solution with various amounts of $K_2TiO(C_2O_4)_2$. The powders were subjected to a final calcination in air at 450 °C for 1 h.

Figure 6 indicates the morphology evolution of thin films synthesized at a fixed $K_2TiO(C_2O_4)_2$ concentration of 50 mM. Only nanowires can be seen within 24 h. Once the reaction duration reached 36 h, a mixed morphology of nanowires and a few nanoflowers were obtained. The amount, as well as the size, of the nanoflowers increased with the prolonged reaction time for up to 72 h. A tentative mechanism can thus be proposed for the

formation of the mixed morphology. Firstly, nanowires were formed by a dissolution-precipitation process according to early researches of our group.[27] After the full development of nanowires, the flower-like rutile mesocrystals nucleated on top of some nanowires, which further grew during the prolonged reaction time.

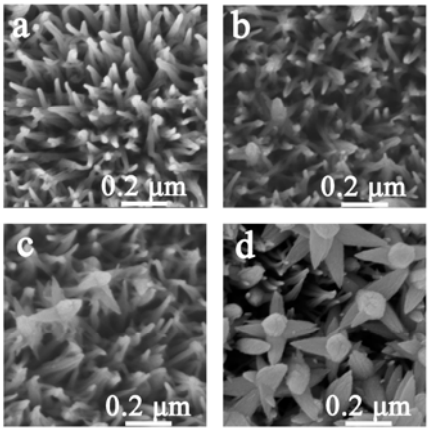

Fig. 6 FESEM morphologies of thin films achieved by the reaction between a Ti plate and the H_2O_2 solution with 50 mM $K_2TiO(C_2O_4)_2$. The reaction duration was (a) 24 h, (b) 36 h, (c) 48 h and (d) 60 h.

The reagent $K_2TiO(C_2O_4)_2$ is composed of Ti atom coordinated by two $[C_2O_4]^{2-}$ ions and bonded by two O atoms, forming octahedral structures which are linked with each other.[28] During the reaction, $[C_2O_4]^{2-}$ in the octahedral structures would be replaced by O_2^{2-} to form an intermediate complex, which would finally decompose to form TiO_2 octahedrons sharing edges, being consistent with the existence of crystalline rutile TiO_2. These TiO_2 octahedrons would self-assemble into petals, which further built up the nanoflowers. In the current investigation, there exists a competition between the formation of pentatitanate nanowires and $K_2TiO(C_2O_4)_2$-induced flower-like rutile mesocrystals. With the additive of 100 mM $K_2TiO(C_2O_4)_2$, the formation of the nanowires was totally inhibited and only nanoflowers were achieved, together with the nanoparticulate aggregates of pentatitanate (**Fig. 3**a). Hong et al. reported that, in an aqueous HNO_3 solution, the homoepitaxial aggregation of ultrathin hydrogen titanate nanowires via a face-to-face oriented attachment, which is accompanied and promoted by a simultaneous phase transformation from the precursor hydrogen titanate to rutile TiO_2, achieved finally rutile TiO_2 mesocrystals.[18a] In the current investigation, it is possible that the additive of $K_2TiO(C_2O_4)_2$ facilitates the procedure, which resulted in the formation of the flower-like rutile TiO_2 mesocrystals.

To clarify the possible effects of K^+, Ti^{4+} and $[C_2O_4]^{2-}$ involved in $K_2TiO(C_2O_4)_2$, reagents of $TiOSO_4$, $K_2C_2O_4$ and $H_2C_2O_4$ have been added to the solution instead of $K_2TiO(C_2O_4)_2$. The additive of $TiOSO_4$ resulted in thin films with a top layer of aligned nanorods (**Fig. 7**a), which is in accordance with Yamabi et al.[29] The nanowires were also obtained upon the additive of either $K_2C_2O_4$ (**Fig. 7**b) or $H_2C_2O_4$ (**Fig. 7**c). The parallel experiment suggests the unique effect of $[TiO(C_2O_4)_2]^{2-}$ in the formation of the present flower-like rutile TiO_2 mesocrystals.

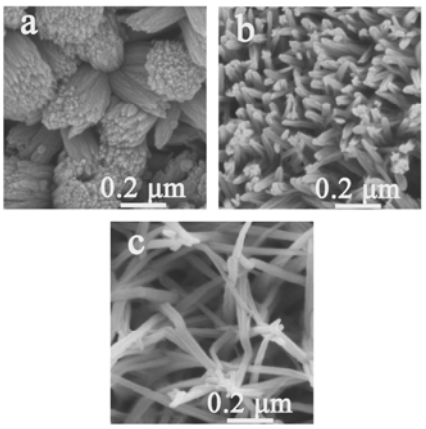

Fig. 7 FESEM morphologies of thin films achieved by the reaction between a Ti plate and the H_2O_2 solution with 100 mM of (a) $TiOSO_4$, (b) $K_2C_2O_4$ and (c) $H_2C_2O_4$.

As illustrated by the UV–Vis spectra (**Fig. 8**a), the nanowire film (0 mM) demonstrated the lowest reflectance, suggesting a higher capability to absorb light when compared with the nanoflowers (100 mM). This can be partly contributed to the much larger film thickness for the nanowire film when compared with the nanoflower film (**Table 1**). The band gap of the nanowire film is determined to be 3.19 eV, larger than the value of 3.08 eV defined for the nanoflower film. The film with the mixed top morphology of nanowires and nanoflowers possessed the lowest band gap of ca. 3.05 eV (50 mM, **Fig. 8**b). Bulk titania possesses a band gap of 3.2 eV for anatase and 3.0 eV for rutile.[30] The reduced band gap values for thin films with rutile nanoflowers are thus reasonable.

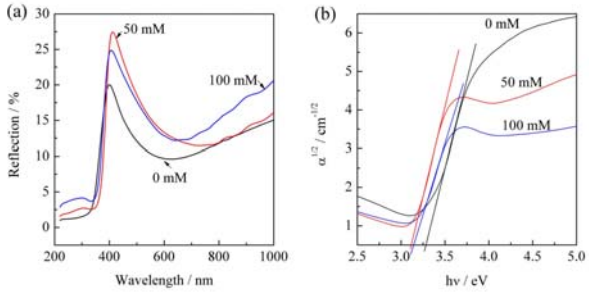

Fig. 8 (a) UV–Vis spectra of thin films achieved by the reaction between a Ti plate and the H_2O_2 solution with various amounts of $K_2TiO(C_2O_4)_2$; (b) re-plotting of (a) in the $\alpha^{1/2}$~hv coordinate to evaluate the corresponding band gap. The films were subjected to a final calcination in air at 450 °C for 1 h.

After calcinations in air at 450 °C for 1 h, both films and powders were utilized to assist photodegradation of SSA under the UV light illumination (**Fig. 9**). All the photocatalysts exhibited negligible SSA absorption within 120 min in dark. For films, nanowires demonstrated remarkably the highest efficiency by decomposing more than 70 % SSA within 120 min. For powders, the result is quite different. All powders showed significant degradation towards SSA within 60 min. The photocatalytic performance was stable for up to 5 cycles, as demonstrated typically in **Fig. 9**c.

Table 1 Band gap and thickness for thin films, low-temperature nitrogen sorption measurement results for powders and the reaction rate constant *k* when utilized to assist photodegradation of sulfosalicylic acid in water. The samples were achieved by the reaction between a Ti plate and the H_2O_2 solution with various amounts of $K_2TiO(C_2O_4)_2$, followed by calcination in air for 1 h at 450 °C.

Concentration of $K_2TiO(C_2O_4)_2$	Band gap eV	Film thickness μm	*k* (films) $\times 10^{-3}$ min^{-1}	Specific surface area m^2 g^{-1}	Pore volume m^3 g^{-1}	Pore diameter nm	*k* (powders) $\times 10^{-3}$ min^{-1}
0 mM	3.19	4.0	5.91	35.59	0.12	3.91	14.7
50 mM	3.05	2.1	1.22	56.21	0.22	3.67	12.1
100 mM	3.08	1.5	2.44	81.15	0.15	3.67	15.9

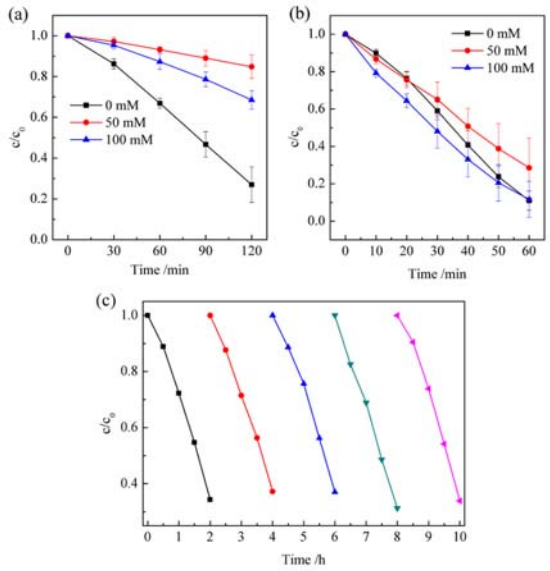

Fig. 9 Photodegradation of sulfosalicylic acid in water in the presence of thin films (a) and powders (b) achieved by the reaction between a Ti plate and the H_2O_2 solution with various amounts of $K_2TiO(C_2O_4)_2$; (c) cycling performance of the nanowire film labelled as 0 mM in (a). The samples were subjected to a final calcination in air at 450 °C for 1 h. The error bar in (a) and (b) was derived by three parallel experiments.

The photodegradation curve can be fitted better into a zero order reaction and the reaction rate constants are summarized in **Table 1**. The anatase nanowire film exhibited the highest efficiency to assist photodegradation of SSA in water, which may be a result of the different film thickness. The slurry system ruled out the effects of film thickness on the photocatalytic activity, which reflects more accurately the inherent efficiency of the various TiO_2. **Fig. 9**b shows similar photocatalytic activity for the powders derived with and without the additive of 100 mM $K_2TiO(C_2O_4)_2$ when utilized in the slurry system. It is commonly accepted that the anatase phase possesses advantageous photocatalytic activity over rutile for photodegradation of most organics, including salicylic acid in water.[31] The powders containing rutile TiO_2 mesocrystals exhibited a photocatalytic activity similar to that of anatase nanowires; it is therefore reasonable to assume that, the rutile TiO_2 mesocrystals favor the photodegradation of SSA in water, thanks to the high specific surface and reduced photo-generated charges inherited from single crystals. Enhanced photocatalytic activity of rutile TiO_2 mesocrystals has also been well documented by Yao[17c] and Aoyama et al.[19]

Under the same condition, the commercial Degussa P25 titania nanoparticles exhibited a reaction rate constant of 39.1 × 10^{-3} min^{-1}, which is much higher than the efficiency of powders achieved in the current investigation. When the P25 nanoparticles were coated on a Ti plate to achieve a film with a load of ca. 1 mg/cm^2 (see Ref. 32 for the coating procedure), which corresponds to a film thickness of ca. 3 μm, the reaction rate constant derived was 5.54×10^{-3} min^{-1}, which is near to that of the nanowire film. The high efficiency in the slurry system can thus be attributed to the well dispersion of P25 in water; however, it is much harder to recover when compared with the present powders.

Conclusions

Flower-like rutile TiO_2 mesocrystals were achieved under a low temperature of 80 °C and the atmospheric pressure through a simple Ti-H_2O_2 reaction. With the additive of $K_2TiO(C_2O_4)_2$ in the reactants, a mixture of hydrogen titanate nanowires and flower-like rutile TiO_2 mesocrystals was achieved. The $K_2TiO(C_2O_4)_2$ reagent is indispensable to the formation of the rutile TiO_2 mesocrystals. After a final calcination in air at 450 °C, the hydrogen titanate nanowires decomposed to anatase TiO_2 nanowires; whilst the rutile TiO_2 mesocrystals remained unchanged. When utilized to assist photodegradation of sulfosalicylic acid under UV illumination, the rutile mesocrystals compensated the inferior photocatalytic activity which is inherent from the rutile phase when compared with anatase, thanks to the unique structure of mesocrystals that possess both high specific surface area and enhanced charge separation rate.

Acknowledgements

This work is supported by the Natural Science Foundation of Zhejiang Province (Project No.: LY13E020001).

Notes and references

[a] *State Key Laboratory of Silicon Materials, Key Laboratory of Advanced Materials and Applications for Batteries of Zhejiang Province and Department of Materials Science and Engineering, Zhejiang University, Hangzhou, 310027, P. R. China. Email: msewjm@zju.edu.cn; Fax: +86-571-87953115; Tel: +86-571-87953115*

1. (a) T. Ohno, K. Sarukawa and M. Matsumura, *J. Phys. Chem. B*, 2001, **105**, 2417; (b) G.F. Lin, J.W. Zheng and R. Xu, *J. Phys. Chem. C*, 2008, **112**, 7363; (c) J. Thomas, K.P. Kumar and S. Mathew, *Sci. Adv. Mater.*, 2011, **3**, 59; (d) J.G. Wang, X.R. Li, X. Li, J. Zhu and H.X. Li, *Nanoscale*, 2013, 5, 1876.
2. A. Fujishima and K. Honda, *Nature*, 1972, **238**, 37.
3. (a) G. Liu, Y.N. Zhao, C.H. Sun, F. Li, G.Q. Lu and H.M. Cheng, *Angew. Chem. Int. Ed.*, 2008, **47**, 4516; (b) S.W. Liu, J.G. Yu and M. Jaroniec, *J. Am. Chem. Soc.*, 2010, **132**, 11914; (c) Y.B. Zhao, F. Pan, H. Li, D.X. Zhao, L. Liu, G.Q. Xu and W. Chen, *J. Phys. Chem. C*, 2013, **117**, 21718; (d) B. Zhao, L. Lin and D.N. He, *J. Mater. Chem. A*, 2013, **1**, 1659.
4. (a) M.M. Ye, Z.L. Chen and W.S. Wang, *J. Hazard. Mater.*, 2010, **184**, 612; (b) Y. Tokunaga, H. Uchiyama, Y. Oaki and H. Imai, *Sci. Adv. Mater.*, 2010, **2**, 69.
5. N, Pugazhenthiran, S. Murugesan and S. Anandan, *J. Hazard. Mater.*, 2013, **263**, 541.
6. (a) B. Li, J.M. Wu, T.T. Guo, M.Z. Tang and W. Wen, *Nanoscale*, 2014, **6**, 3046; (b) D.W. Chu, Y.P. Zeng, D.L. Jiang and Y. Masuda, *Sci. Adv. Mater*., 2009, **1**, 227.
7. F.L. Su, T. Wang, R. Lv, J.J. Zhang, P. Zhang, J.W. Lu and J.L. Gong, *Nanoscale*, 2013, **5**, 9001.
8. F. Li, J. Xu, L. Chen, B.B. Ni, X.N. Li, Z.P. Fu and Y.L. Lu, *J. Mater. Chem. A*, 2013, **1**, 22.
9. Q. Guo, X.M. Wu, Y.M. Fan and X.Y. Zhou, *J. Alloys Compd.*, 2013, **579**, 322.
10. (a) Z.A. Huang, Z.Y. Wang, K.L. Lv, Y. Zheng and K.J. Deng, *ACS Appl. Mater. Interfaces*, 2013, **5**, 8663; (b) A.M. Bakhshayesh, M.R. Mohammadi, H. Dadar and D.J. Fray, *Electrochim. Acta*, 2013, **90**, 302.
11. H. Colfen and M. Antonietti, *Angew. Chem. Int. Ed.*, 2005, **44**, 5576.
12. (a) J.H. Zhao, R.Q. Tan, Y.Q. Guo, Y.H. Lu, W. Xu and W.J. Song, *CrystEngComm*, 2012, **14**, 4575; (b) Z.H. Li, A. Geβner, J.P. Richters, J. Kalden, T. Voss, C. Kubel and A. Taubert, *Adv. Mater.*, 2008, **20**, 1279.
13. (a) Y.B. Cao, J.M. Fan, L.Y. Bai, P. Hu, G. Yang, F.L. Yuan and Y.F. Chen, *CrystEngComm*, 2010, **12**, 3894; (b) T. Li, H.J. You, M.W. Xu, X.P. Song and J.X. Fang, *ACS Appl. Mater. Interfaces*, 2012, **4**, 6942.
14. Y. Zhao, Y. Lu, Y. Hu, J.P. Li, L. Dong, L.N. Lin and S.H. Yu, *Small*, 2010, **21**, 2436.
15. F.C. Meldrum and H. Colfen, *Chem. Rev.*, 2008, **108**, 4332.
16. (a) S.J. Liu, J.Y. Gong, B. Hu and S.H. Yu, *Cryst. Growth Des*., 2009, **9**, 203; (b) W. Jiao, L.Z. Wang, G. Liu, G. Q. Lu and H.M. Cheng, *ACS catal.*, 2012, **2**, 1854; (c) H. Wang, Y. Liu, Z. Liu, H.M. Xu, Y.J. Deng and H. Shen, *CrystEngComm*, 2012, **14**, 2278; (d) J.G. Cai, J.F. Ye, S.Y. Chen, X.W. Zhao, D.Y. Zhang, S. Chen, Y.R. Ma, S. Jin and L.M. Qi, *Energy Environ. Sci.*, 2012, **5**, 7575; (e) P. Gao, J.C. Liu, T. Zhang, D.D. Sun and W. Ng, *J. Hazard. Mater.*, 2012, **229-230**, 209.
17. (a) L. Li and C.Y. Liu, *CrystEngComm*, 2010, **12**, 2073; (b) Q.F. Chen, W.H. Ma, C.C. Chen, H.W. Ji and J.C. Zhao, *Chem. Eur. J.*, 2012, **18**, 12584; (c) X.X. Yao, X.H. Liu, T.Y. Liu, K. Wang and L.D. Lu, *CrystEngComm*, 2013, **15**, 10246; (d) X.F. Yang, J.L. Qin, Y. Li, R.X. Zhang and H. Tang, *J. Hazard. Mater.*, 2013, **261**, 342; (e) J.Y. Feng, M.C. Yin, Z.Q. Wang, S.C. Yan, L.J. Wan, Z.S. Li and Z.G. Zhou, *CrystEngComm*, 2010, **12**, 3425; (f) J.F. Ye, W. Liu, J.G. Cai, S. Chen, X.W. Zhao, H.H. Zhou and L.M. Qi, *J. Am. Chem. Soc.*, 2011, **133**, 933.
18. (a) Z.S. Hong, M.D. Wei, T.B. Lan, L.L. Jiang and G.Z. Cao, *Energy Environ. Sci.*, 2012, **5**, 5408; (b) Z.S. Hong, Y.X. Xu, Y.B. Liu and M.D. Wei, *Chem. Eur. J.*, 2012, **18**, 1075; (c) Z.S. Hong, M.D. Wei, T.B. Lan and G.Z. Cao, *Nano Energy*, 2012, **1**, 466.
19. Y. Aoyama, Y. Oaki, R. Ise and H. Imai, *CrystEngComm*, 2012, **14**, 1405.
20. R. D. Silva, R.H. Goncalves, D.G. Stroppa, A.J. Ramirez and E.R. Leite, *Nanoscale*, 2011, **3**, 1910.
21. (a) X.C. Jiang, T. Herricks and Y.N. Xia, *Adv. Mater*., 2003, **15**, 17; (b) X.C. Jiang, Y.L. Wang, T. Herricks and Y.N. Xia, *J. Mater. Chem*., 2004, **14**, 695; (c) G. Cheng, M.S. Akhtar, O.B. Yang and F.J. Stadler, *Electrochim. Acta*, 2013, **113**, 527; (d) G. Cheng, M.S. Akhtar, O.B. Yang and F.J. Stadler, *ACS Appl. Mater. Interfaces*, 2013, **5**, 6635.
22. J.M. Wu, Y.Q. Zhang, H.X. Xue, G.H. Bai, L.L. Lai and M.Z. Tang, *Sci. Adv. Mater*., 2012, **4**, 719.
23. (a) L. Zhou, D.S. Boyle and P. O'Brien, *Chem. Commun.*, 2007, **2**, 144; (b) L. Zhou, D.S. Boyle and P. O'Brien, *J. Am. Chem. Soc.*, 2008, **130**, 1309; (c) Z.F. Bian, T. Tachikawa and T. Majima, *J. Phys. Chem. Lett.*, 2012, **3**, 1422.
24. J. Sun and J.M. Wu, *Adv. Sci. Mater*. 2013, **5**, 1.
25. W.X. Guo, C. Xu, X. Wang, S.H. Wang, C.F. Pan, C.J. Lin and Z.L. Wang, *J. Am. Chem. Soc.*, 2012, **134**, 4437.
26. J.S. Chen, Y.L. Tan, C.M. Li, Y.L. Cheah, D. Luan, S. Madhavi, F.Y. Boey, L.A. Archer and X.W. Lou, *J. Am. Chem. Soc.*, 2010, **132**, 6124.
27. J.M. Wu and H.X. Xue, *J Am. Ceram. Soc.*, 2009, **92**, 2139.
28. X.X. Li, Y.J. Xiong, Z.Q. Li and Y. Xie, *Inorg. Chem.*, 2006, **45**, 3493.
29. S. Yamabi and H. Imai, *Chem. Mater.*, 2002, **14**, 609.
30. Y.C. Lan, Y.L. Lu and Z.F. Ren, *Nano Energy*, 2013, **2**, 1031.
31. Z. Ambrus, K. Mogyorósi, Á. Szalai, T. Alapi, K. Demeter, A. Dombi and P. Sipos, *Appl. Catal. A*, 2008, **340**, 153.
32. J.M. Wu, T.W. Zhang, Y.W. Zeng, S. Hayakawa, T. Kanji and A. Osaka, *Langmuir*, 2005, **21**, 6995.

Table of Contents Entry

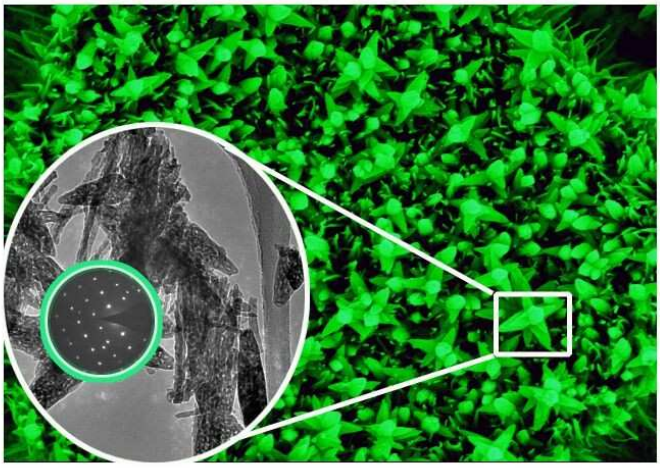

Flower-like rutile TiO_2 mesocrystals were synthesized by a $K_2TiO(C_2O_4)_2$-mediated low temperature solution route under the atmospheric pressure, which exhibited high photocatalytic activity because of the large specific surface area as well as the high charge separation rate inherent from the single crystal nature.